

Photometric Properties of the Arp 220 Super Star Clusters

Yasuhiro Shioya^{1*}, Yoshiaki Taniguchi¹, & Neil Trentham²

¹*Astronomical Institute, Graduate School of Science, Tohoku University, Aramaki, Aoba, Sendai 980-8578, Japan*

²*Institute of Astronomy, University of Cambridge, Madingley Road, Cambridge CB3 0HA, UK*

22 October 2018

ABSTRACT

We investigate the photometric properties of six super stellar clusters (SSCs) seen in both the optical and near-infrared Hubble Space Telescope images of the local ultraluminous starburst galaxy Arp 220. Three of the SSCs are located in the central 0.5 kpc region. The remaining three are in the circumnuclear region between 0.5 kpc and 2.5 kpc from the centre. Comparing the observed spectral energy distributions (SEDs) of the SSCs with the Starburst99 models of Leitherer et al., we confirm that all the three nuclear SSCs are heavily obscured ($A_V \sim 10$ mag). Considering the results from this comparison in conjunction with measurements of the near-infrared CO absorption index and of millimetre CO line widths and luminosities, we estimate the ages of the nuclear SSCs to be $10^7 - 10^8$ yrs. The bolometric luminosity of the three nuclear SSCs is at most one-fifth of the total bolometric luminosity of Arp 220. On the other hand, the circumnuclear SSCs have little internal extinction ($A_V \leq 1$ mag). These contribute negligibly to the total bolometric luminosity.

Key words: galaxies: individual (Arp 220) – galaxies: starburst – stars: formation

1 INTRODUCTION

Ultraluminous infrared galaxies (ULIGs) are the most luminous objects in the local universe (their bolometric luminosities $> 10^{12}L_\odot$). The ULIGs are undergoing major dissipative collapses, which are probably triggered by mergers (Clements et al. 1996; Murphy et al. 1996).

Whether the ULIGs are powered by starbursts or active galactic nuclei (AGN) has remained unknown since their discovery because of huge amounts of internal extinction along our lines of sight to their centres (for a review see Sanders & Mirabel 1996). However, recent mid-infrared spectroscopic work (Genzel et al. 1998) suggests that the major energy sources of most local ULIGs are nuclear starbursts. This provides an important motivation for studying the star formation in the centres of ULIGs in detail.

The nearest and best-studied ULIG is the star-forming (Genzel et al. 1998) galaxy Arp 220 (far-infrared luminosity $1.5 \times 10^{12}L_\odot$) at a distance of 74 Mpc (assuming $H_0 = 75$ km s⁻¹ Mpc⁻¹ and $\Omega_0 = 1$; de Vaucouleurs et al. 1991). Detailed imaging of the centre of Arp 220 with the *Hubble Space Telescope* has revealed a number of super star clusters (SSCs; Shaya et al. 1994; Scoville et al. 1998). These nuclear SSCs appear to be a generic feature of luminous merging galaxies (Lutz 1991; Ashman & Zepf 1992; Holtzman et al. 1992; Zepf & Ashman 1993; Surace et al. 1998; Surace &

Sanders 1999). Surace et al. (1998) and Surace & Sanders (1999) evaluated the luminosities of SSCs in warm ULIGs and concluded that the combined contributions of the all the individual detected circumnuclear SSCs to the bolometric luminosities are small. They also showed that for some warm ULIGs the de-reddened luminosities of putative nuclei are not able to account for the bolometric luminosity and that a large fraction of the bolometric luminosity must arise from sources undetected at both optical and near-infrared wavelengths.

In this paper, we compare the observed optical and near-infrared spectral energy distributions (SEDs) of the Arp 220 SSCs with the Starburst99 model SEDs of Leitherer et al. (1999) and estimate their ages, masses, and luminosities, along with the internal extinction along our lines of sight to them. This is the first attempt to analyse by SED fitting methods the properties of SSCs in the centre of Arp 220, which is colder (Sanders et al. 1988) than the ULIGs studied by Surace et al. (1998). These results will let us evaluate how much of the very substantial amount of star formation currently happening in Arp 220 is in the SSCs, at least in the ones which are not completely invisible at optical and near-infrared wavelengths due to internal extinction. Recently, Soifer et al. (1999) presented the images of Arp 220 from 3.45 to 24.5 μm . Since Genzel et al. (1998) derived the value of $A_V = 45$ mag based on the mid-infrared hydrogen recombination lines (Br β λ 2.17 μm , Br α λ 4.05 μm and Pf α λ 7.46 μm), the mid-infrared sources observed by Soifer et al. (1999) must be highly obscured objects. This

* shioya@astr.tohoku.ac.jp

suggests that what Surace et al. (1998) found to be true in the warm ULIGs, specifically that the contribution of the observed clusters to the bolometric luminosity is small, is also true in Arp 220. We now investigate this in detail by studying the energy outputs of the SSCs themselves.

2 METHODS

2.1 Identifications of SSCs

The *Hubble Space Telescope* images of the core of Arp 220 show eleven SSCs at optical (V -, R -, and I -band) wavelengths (Shaya et al. 1994) and twelve SSCs at near-infrared (J -, H -, and K -band) wavelengths (Scoville et al. 1998). In this paper, we call the F110W filter ($1.1\ \mu\text{m}$) as J filter, though the standard J filter is at $1.25\ \mu\text{m}$. We combine these datasets in order to obtain a set of SSCs that are detected at all wavelengths. This allows us to sample the SEDs over as wide a range in wavelength as possible.

Three SSCs are located in the outer regions of the core – we expect dust extinction to be smallest here, so that these SSCs should be seen at all wavelengths. Given the published coordinates, there is a slight offset between the near-infrared and optical positions of these SSCs (see the left panel of Figure 1). However, if we rotate the near-infrared images by -4° around the nuclear SSC associated with the western nucleus, the positions of the star clusters in the two images are almost coincident (see the right panel of Figure 1). Given the probable low extinction along these lines of sight, we regard this astrometrical solution as likely to be the correct one. In addition, given this astrometry, we then find that three nuclear SSCs (hereafter N1, N2, and N3) are coincident in the optical and near-infrared images, in addition to the three circumnuclear ones (hereafter C1, C2, and C3).

2.2 Spectral energy distributions of the SSCs

In Figure 2, we show the observed SEDs of the six SSCs. We use the photometric data published by Shaya et al. (1994; VRI bands) and by Scoville et al. (1998; JHK bands) for SSC N2 – N3 and C1 – C3. In the case of SSC N1, we have used *HST* archival data to measure the optical fluxes using the same $0.92\ \text{arcsec} \times 0.58\ \text{arcsec}$ aperture used by Scoville et al. (1998) for the near-infrared measurements (Shaya et al. used a smaller aperture in their analysis). The magnitudes of SSC N1 are 21.96 mag and 19.36 for R -band (F702W) and I -band (F785LP) respectively. This SSC was not detected in the V -band (F555W).

All three nuclear SSCs show a peak at $1.6\ \mu\text{m}$, whereas all three circumnuclear SSCs have SEDs that rise towards bluer wavelengths. This is a very important difference and is immediately suggestive of far more dust extinction along the lines of sight to the nuclear SSCs than along the lines of sight to the circumnuclear ones.

We now compare the SEDs with the Starburst99 spectral synthesis models of Leitherer et al. (1999). One of the advantages of the Starburst99 is that it tell us the evolution of the strength of CO index which is useful to constrain the range of ages. When fitting model SEDs to observed ones in

the presence of internal extinction, there are several parameters that we need to consider:

1) the mode of star formation. For example, the star formation may occur continuously (the constant star formation, or CSF model), may occur in a short, almost instantaneous, burst (the instantaneous starburst, or ISB model), or may occur in a way that varies with time in a complex manner. For the blue circumnuclear SSCs, there is no evidence that star formation has been ongoing in these isolated clusters for any considerable time, and we adopt an ISB model for describing star formation in these systems. On the other hand, the nuclear star-forming regions of Arp 220 are probably at least 10^8 years old (Mouri & Taniguchi 1992; Prestwich, Joseph, & Wright 1994; Armus et al. 1995; Larkin et al. 1995). Yet there still appear to be ionizing sources in the nuclear region (Larkin et al. 1995, Kim et al. 1995, and Goldader et al. 1995). Therefore an ISB model will not work here, and we approximate star formation in the nuclear SSCs by a CSF model. On the other hand, there is a possibility that the nuclear SSCs are not the ongoing starburst discussed in the above papers but post-starburst and we also consider an ISB model for the nuclear SSCs, although we regard the CSF one as the more likely;

2) the stellar IMF. We adopt a Salpeter IMF with an upper mass cutoff of $M_{\text{u}} = 100 M_{\odot}$ and a lower mass cutoff of $M_{\text{l}} = 1 M_{\odot}$. We note that M_{l} might be larger in a violent star-forming region (see e.g. Goldader et al. 1997) and investigate the effect of the IMF on our results in the next section;

3) the initial gas metallicity. We assume solar metallicity ($Z = 0.02$). Since the metallicity of galactic centre may be larger than the solar value, we also study the case of $Z = 0.04$ (see the next section);

4) the age at which we observe the star clusters. We leave this as a free parameter in the range of $2 \times 10^5\ \text{yr}$ to $1 \times 10^9\ \text{yr}$;

5) the effect of extinction. The total extinction can be regarded as the sum of two parts: 1) extinction from dust in Arp 220 along our line of sight to the SSCs, and 2) extinction from dust *within* the SSCs. The relative importance of these two regimes can be tested as follows. A screen model may be used to describe extinction along our line of sight to the SSCs, and the “onion-skin” model of Surace and Sanders (1999) may be used to quantify the extinction from dust within the SSCs. This comparison is made in Appendix A, where we show that (1) is the more important regime. We consequently adopt a screen model and leave the absolute value A_V of the extinction in the V -band as a free parameter to be fit to the data, but impose the constraint that the extinction must vary with wavelength according to the extinction curve of Cardelli et al. (1989);

6) nebular emission. Starburst99 includes the nebular continuum emission which is proportional to the flux of ionizing photons. If all of the Lyman continuum photons are used to ionize the surrounding gas, the equivalent width of $H\alpha$ can reach $1000\ \text{\AA}$ and the R -band flux becomes twice as large as that from the continuum. However, the *measured* equivalent width of the $H\alpha$ emission line in Arp 220 is only $20 - 30\ \text{\AA}$ (Armus et al. 1989, Veilleux et al. 1995). If the equivalent width of $H\alpha$ emission of each SSC is the same as the total ones, the contribution of emission lines to the broadband photometry is then negligibly small. We neglect it here;

7) dust emission. Hot dust emission was required to interpret a K -band flux excess in previous studies (Surace & Sanders 1999 for warm ULIGs; Mazzarella et al. 1992 for the nuclei of Arp 220). However, there is little K -band flux excess for our sample. We ignore the hot dust emission in our models.

Using maximum likelihood techniques, we determine the best-fitting model SEDs to the observed ones for the six SSCs. The likelihood is defined as

$$L = \prod_i^6 \exp \left\{ -\frac{1}{2} \left[\frac{F_{o,i} - a \cdot F_{m,i}}{\sigma_i} \right]^2 \right\} \quad (1)$$

where $F_{o,i}$, $F_{m,i}$ and σ_i are the observed flux, the template flux, and the uncertainty of the observed flux of i -th band. The uncertainty of the photometry we adopted is ± 0.4 mag for Shaya et al. (1994) and ± 0.1 mag for Scoville et al. (1998). A scale factor a is obtained as

$$a = \frac{\sum_{i=1}^6 F_{m,i} F_{o,i} / \sigma_i^2}{\sum_{i=1}^6 (F_{m,i})^2 / \sigma_i^2} \quad (2)$$

from the condition of $\partial L / \partial a = 0$. The results are summarized in Table 1 and the SEDs of best-fitting models are presented in Figure 2.

3 RESULTS AND DISCUSSION

3.1 Properties of the nuclear SSCs

Figure 3 is a summary of the region of plausible parameters in the A_V - age plane for the nuclear SSCs. The results for the CSF model are shown in figure 3 (a) - (c) and those for the ISB model are shown in figure 3 (d) - (f).

The hatched region is the region of plausible parameters at the 99 % confidence level. We immediately see that the extinction A_V along our lines of sight to the nuclear SSCs is very large (~ 10 mag). These values are slightly larger than those evaluated by Shaya et al. (1994) while slightly smaller than those of Scoville et al. (1998). These differences can be attributed to the extinction curves adopted in the analyses [Shaya et al. use the extinction curve of Savage & Mathis (1979), while Scoville et al. use that of Rieke & Lebofsky (1985)].

On the other hand, it is difficult to determine the age of SSCs, due to strong parameter coupling with the extinction. A small change in A_V mimics a substantial change in age in the sense that both shift the SED towards redder wavelengths.

We explain the rough shapes of the relevant parameter space as follows. If the stellar populations are very young (age $< 10^7$ yr), A_V must be very large, since the intrinsic slope of the continuum is very blue and a great deal of extinction is required to make it as red as is observed. For stellar populations older than several $\times 10^7$ yr, the allowed values of A_V do not vary strongly with age since the slope of continuum does not vary with the age of the stars. At the age of $\sim 10^7$ yr in the ISB model, the plausible value of A_V becomes small temporarily due to the presence of a large number of red supergiants at exactly this age.

Therefore, we cannot determine the ages of the nuclear SSCs this way. We must use additional measurements. For N1, there exists an independent constraint on the mass of the SSC from radio and millimetre observations. The mass of N1 as determined by the SED fit represents a locus of points in the A_V -age plane, and is shown in Figure 3 (the dashed line).

The position of N1 corresponds to the western nucleus observed to exhibit radio continuum, 1.3 mm dust continuum and the CO (1-0) and (2-1) lines (Scoville et al. 1997; Downes & Solomon 1998; Sakamoto et al. 1999). Millimetre spectroscopy (of CO lines) can be used to determine both a dynamical mass (from the line widths) and a molecular gas mass (from the line luminosities). From the results of Downes & Solomon (1998) and Sakamoto et al. (1999), we estimate a dynamical mass of this nucleus of $2 \times 10^9 M_\odot$ and a gas mass of $1 \times 10^9 M_\odot$ [adopting the inclination parameter of Scoville et al. (1998)]. The mass of the stellar component must be less than the difference between these two masses, which is $1 \times 10^9 M_\odot$. If there are other (highly obscured) stellar components present within the region, this number is an upper limit; if all the mass of N1 is in gas and observed stars, then this is an equality. The dashed lines in figure 3 (a) and (d) show the locus of SSCs with the mass of $1 \times 10^9 M_\odot$. The region of plausible parameters is now restricted to that to the left of the lines. The upper limits on the age of N1 are now 2.0×10^8 yr for the CSF model and 5.0×10^7 yr for the ISB model. The reason why we can set an upper limit of age is that the luminosity-to-mass ratio of the stellar cluster becomes smaller as it gets older and consequently a more massive cluster is required to radiate the observed flux.

The dynamical masses of N2 and N3 have not been measured. Although the eastern nucleus of Arp 220 has been detected in CO, the position of it corresponds to neither N2 nor N3. Instead it is an entirely different object (hereafter we call it as N4), coincident with the nuclear source SE in the near-infrared images of Scoville et al. (1998). Based on the fact that N1 and N4 only exhibit non-thermal radio continuum, thermal dust continuum, and molecular gas, Scoville et al. (1998) suggested that these two objects represent the most substantial mass concentrations in the centre of Arp 220.

We now consider yet another way to constrain the range of ages of the nuclear SSCs. The strength of CO absorption index at $2.29 \mu\text{m}$ constrains the ages since it is sensitive primarily to the presence of red K supergiants, which are stars with a narrow age distribution, particularly in the ISB models. The CO index of the centre of Arp 220 is known to be strong: 0.24 ± 0.01 mag (Goldader et al. 1995), 0.20 ± 0.05 mag (Shier et al. 1996), and > 0.20 mag [Armus et al. (1995) for the central 0.7×2 arcsec 2]. Although the CO indices of each SSC are not individually observed, if we assume that all three nuclear SSCs have a CO index larger than 0.20 mag, then we get following additional constraint on the ages: $8.1 \times 10^6 \leq \text{age/yr} \leq 4.5 \times 10^7$ for the ISB model, or $1.2 \times 10^7 \leq \text{age/yr} < 1.2 \times 10^8$ for the CSF model. In the case of the ISB model, the CO index is 0 mag until the age of 7.1×10^6 yr and become strong rapidly at later times, reaching 0.2 mag at the age of 8.0×10^6 yr, which corresponds to the main-sequence lifetime of the stars with mass of $25 M_\odot$, the main progenitors of the K supergiants. After that, the CO index decreases gradually and becomes

smaller than 0.2 mag at 4.5×10^7 yr. In the case of the CSF model, since newly formed red supergiants keep the CO index strong, the CO index continues to be larger than 0.2 mag for a longer time than for the ISB model. The strength of the CO index is modified slightly by dust as follows. Since the continuum level is determined on the blue side of CO band, dust extinction has the effect of causing us to underestimate the continuum and therefore to underestimate the CO index. Ignoring dust emission at 2.3 microns has the same effect since the SED of the dust component is rising towards longer wavelengths. If the intrinsic value of CO index is larger than we think, then the upper limit of the age of SSCs become smaller. Ignoring the effects of dust therefore does not invalidate the upper limits we present.

Rieke et al. (1985) reported that the equivalent width of H β absorption within the central 2.5 arcsec of Arp 220 is 4 Å. This value of the Balmer absorption is incompatible with such a strong CO index for single stellar cluster. Probably this discrepancy arises because the Balmer feature originates from old foreground (possibly progenitor galaxy) stars that happen to lie at low optical depth and are quite unrelated to the SSCs. The flux of the nuclear region of Arp 220 at very blue wavelengths is therefore likely to be dominated by foreground stars at low skin-depth. Recall that the nuclear SSCs were not observed in the *V*-band so the extinction at these short wavelengths is probably quite high.

We can now estimate the maximum bolometric luminosity emitted from the nuclear star clusters from the above results. For the ISB model, the maximum bolometric luminosities of N1, N2, N3 are $1.0 \times 10^{11}L_{\odot}$, $1.2 \times 10^{10}L_{\odot}$ and $4.1 \times 10^{10}L_{\odot}$. The sum of these luminosities is $1.5 \times 10^{11}L_{\odot}$ which is about one-tenth of the bolometric luminosity of Arp 220 ($1.5 \times 10^{12}L_{\odot}$, Sanders et al. 1988). For the CSF model, the maximum bolometric luminosities of N1, N2, N3 are $1.9 \times 10^{11}L_{\odot}$, $2.2 \times 10^{10}L_{\odot}$ and $7.6 \times 10^{10}L_{\odot}$. The sum of these is $2.9 \times 10^{11}L_{\odot}$ which is about one-fifth of the bolometric luminosity of Arp 220. We can therefore state with some confidence that if most of the total bolometric luminosity of Arp 220 arises from the nucleus, more than four-fifths of it arises from highly obscured starbursts (or possibly an AGN).

The results depend on the IMF as follows. A steeper IMF decreases the implied ages of the star clusters. For example, IMF with ($\alpha = 3.30$, $M_u = 100M_{\odot}$, $M_l = 1M_{\odot}$) decreases the maximum ages derived from the stellar mass ($< 10^9M_{\odot}$) to 1.6×10^7 yr for the CSF model or 1.4×10^7 yr for the ISB model. On the other hand, a truncated IMF increases the ages. For example, an IMF with ($\alpha = 2.35$, $M_u = 30M_{\odot}$, and $M_l = 1M_{\odot}$) increases the upper limits on the ages to 2.4×10^8 yr for the CSF model and 5.2×10^7 yr for the ISB model. The evolution of CO index also depends on the IMF, since the number of red supergiants per unit total stellar mass at any time is a function of the IMF. If we adopt the steeper IMF as above, the range of ages when the CO index is larger than 0.2 mag is $1.1 \times 10^7 \leq \text{age/yr} \leq 7.1 \times 10^7$ for the CSF model or $8.2 \times 10^6 \leq \text{age/yr} \leq 3.6 \times 10^7$ for ISB model. For the truncated IMF, it is $1.0 \times 10^7 \leq \text{age/yr} \leq 1.6 \times 10^8$ for the CSF model or $8.1 \times 10^6 \leq \text{age/yr} \leq 4.5 \times 10^7$ for the ISB model. The bolometric luminosity emitted from the nuclear star clusters also depends on the IMF, since we have imposed a constraint on the mass. The bolometric luminos-

ity ranges between $2.9 \times 10^{11}L_{\odot}$ (CSF model with standard IMF) and $1.4 \times 10^{11}L_{\odot}$ (ISB model with steeper IMF); the basic conclusions are unchanged.

The metallicities of many luminous elliptical galaxies (the probable fate of ultraluminous galaxies like Arp 220) are often considerably higher than solar (Faber 1973). It is therefore important to investigate how the results change if the metallicity is increased to twice solar (section 3.1, p.10), comparable to the values in the most luminous ellipticals (Faber 1973). For the SED fitting, the larger metallicity causes only a very small change, but the length of time when the CO index is strong is considerably longer. The range of ages when the CO index is larger than 0.2 mag is $8.5 \times 10^6 \leq \text{age/yr} \leq 3.0 \times 10^8$ for the CSF model or $6.9 \times 10^6 \leq \text{age/yr} \leq 5.4 \times 10^7$ for the ISB model. The maximum bolometric luminosities are $3.4 \times 10^{11}L_{\odot}$ for CSF model and $1.0 \times 10^{11}L_{\odot}$ for ISB model; the basic conclusions are also unchanged.

It is also useful to estimate how much of the difference between the total bolometric luminosities and the luminosities of the observed SSCs can be made up if one includes the contribution from N4, the SE nucleus seen in the near-infrared but not the optical images. From SED fitting, we derive a value of $A_V \sim 12$ mag (Figure 4), much smaller than the value of $A_V \sim 20$ mag evaluated by Scoville et al. (1998). This discrepancy comes from the fact that we use all three of the *J*-, *H*-, and *K*- band fluxes for SED fitting, whereas Scoville et al. use only the *H* – *K* colour.

If, as for N1, we assume that the maximal mass of N4 is the dynamical mass minus the gas mass, and assume that the strength of the CO index is greater than 0.2 mag, we derive a maximum intrinsic luminosity of N4 of $2.0 \times 10^{10}L_{\odot}$ for ISB model or $3.7 \times 10^{10}L_{\odot}$ for CSF model.

Adding these values to the summation of the bolometric luminosities of N1 - N3, we derive a maximum bolometric luminosity emitted from the nuclear SSCs of $1.73 \times 10^{11}L_{\odot}$ for the ISB model and $3.22 \times 10^{11}L_{\odot}$ for the CSF model. These values are still much smaller than the total bolometric luminosity of Arp 220. Again, this result is essentially not affected by the IMF or metallicity.

Therefore the conclusion that most of the bolometric luminosity we see originating from the nucleus of Arp 220 comes from heavily obscured star formation seems unavoidable. At optical and near-infrared wavelengths we see only a small fraction (less than one-fifth) of it. The fact that the total luminosity of observed sources cannot account for the bolometric luminosity is similar to those derived for the putative nuclei of warm ULIGs (Surace & Sanders 1999).

3.2 Properties of the circumnuclear SSCs

Figures 3 (g) - (i) summarize the allowed regions on the A_V - age plane for the circumnuclear SSCs. The data require total extinctions of $A_V < 1$ mag, far less than for the nuclear SSCs. Because of this low extinction, the cluster ages, masses, and luminosities are much better constrained by the SED fits than for the nuclear clusters. We find that the upper limits on the ages of the SSCs are 2.0×10^6 yr, 4.6×10^8 yr, and 8.4×10^8 yr for C1, C2 and C3. These results are very different from those of Scoville et al. (1998), who suggests that they may be as old as ($\gtrsim 10^9$ years) the central

globular clusters of NGC 5128 (Frogel 1984), because of the similarity of near-infrared colours. We attribute this slight redness of the star clusters to a little amount of dust rather than to a very large age. We also mention that since the near-infrared colours of star clusters mainly depend on the colours of red supergiants and red giants, the evolution of near-infrared colours is small for the age larger than $\sim 10^7$ yr. On the other hand, the optical colours, which mainly determined by the colours of the upper main sequence stars, evolve gradually from blue to red for the Hubble time. It is therefore useful to use the optical colours to determine the age of SSCs.

We summarize the best-fitting parameters for the circumnuclear SSCs in Table 1. The masses of the SSCs are about $10^5 M_{\odot}$, similar to the masses of galactic globular clusters. Maybe these are the globular clusters hypothesized to form during mergers by Zepf & Ashman (1993), who note that elliptical galaxies (thought to be merger remnants) have higher specific globular cluster frequencies than spiral galaxies (thought to be merger progenitors), and that the metallicity distributions of the globular clusters in the ellipticals are bimodal. The luminosities of the SSCs are about $10^8 L_{\odot}$. Therefore C1 - 3 contribute negligibly to the total bolometric luminosity of Arp 220. This result is unchanged if we consider the other circumnuclear SSCs which are detected only at near-infrared wavelengths.

We would like to thank Bob Joseph for his useful comments and suggestions on an earlier version of our manuscript. YS thanks the Japan Society for Promotion of Science (JSPS) Research Fellowships for Young Scientist. NT thanks the PPARC for financial support. This work was financially supported in part by Grant-in-Aids for the Scientific Research (Nos. 07044054, 10044052, and 10304013) of the Japanese Ministry of Education, Science, Sports and Culture.

REFERENCES

- Armus L., Heckman T. M., Miley G. K. 1989, *ApJ*, 347, 727
 Armus L., Neugebauer G., Soifer B. T., Matthews K. 1995, *AJ*, 110, 2610
 Ashman K. M., Zepf S. E. 1992, *ApJ*, 384, 50
 Baan W. A., Haschick A. D. 1995, *ApJ*, 454, 745
 Cardelli J. A., Clayton G. C., Mathis J. S. 1989, *ApJ*, 345, 245
 Clements D. L., Sutherland W. J., McMahon R. G., & Saunders W. 1996, *MNRAS*, 279, 477
 de Vaucouleurs G., de Vaucouleurs A., Corwin H. G., Jr., Buta R. J., Paturel G., Forqu e P. 1991, *Third Reference Catalogue of Bright Galaxies* (Springer-Verlag)
 Downes D., Solomon P. M. 1998, *ApJ*, 507, 615
 Faber S. M. 1973, *ApJ*, 179, 731
 Genzel R. et al. 1998, *ApJ*, 498, 579
 Goldader J. D., Joseph R. D., Doyon R., Sanders, D. B. 1995, *ApJ*, 444, 97
 Goldader J. D., Joseph R. D., Doyon R., Sanders D. B. 1997, *ApJS*, 108, 449
 Holtzman J. A., et al. 1992, *AJ*, 103, 691
 Kim D.-C., Sanders D. B., Veilleux S., Mazzarella J. M., Soifer B. T. 1995, *ApJS*, 98, 171
 Larkin J. E., Armus L., Knop K., Matthews K., Soifer, B. T. 1995, *ApJ*, 452, 599
 Leitherer C. et al. 1999, *ApJS*, 123, 3
 Lutz D. 1991, *A & A*, 245, 31
 Mouri H., Taniguchi Y. 1992, *ApJ*, 386, 68
 Murphy T. W., Armus L., Matthews K., Soifer B. T., Mazzarella J. M. 1996, *AJ*, 111, 1025
 Prestwich A. H., Joseph R. D., Wright G. S. 1994, *ApJ*, 422, 73
 Rieke G. H., Cutri R. M., Black J. H., Kailey W. F., McAlary C. W., Lebofsky M. J., Elston R. 1985, *ApJ*, 290, 116
 Rieke G. H., Lebofsky M. J. 1985, *ApJ*, 288, 618
 Sakamoto K., Scoville N. Z., Yun M. S., Crosas M., Genzel R., Tacconi L. J. 1999, *ApJ*, 514, 77
 Sanders D. B., Mirabel I. F. 1996, *ARA & A*, 34, 749
 Sanders D. B., Soifer B. T., Elias J. H., Madore B. F., Matthews K., Neugebauer G., Scoville N. Z. 1988, *ApJ*, 325, 74
 Savage B. D., Mathis J. S. 1979, *ARA&A*, 17, 73
 Scoville N. Z. et al. 1998, *ApJ*, 492, L107
 Scoville N. Z., Sargent A. I., Sanders D. B., Soifer B. T. 1991, *ApJ*, 366, L5
 Scoville N. Z., Yun M. S., Bryant P. M. 1997, *ApJ*, 484, 702
 Shaya E., Dowling D. M., Currie D. G., Faber S. M., Groth E. J. 1994, *AJ*, 107, 1675
 Soifer B. T., Neugebauer G., Matthews K., Becklin E. E., Ressler M., Werner M. W., Weinberger A. J., Egami E. 1999, *ApJ*, 513, 207
 Surace J. A., Sanders D. B. 1999, *ApJ*, 512, 162
 Surace J. A., Sanders D. B., Vacca W. D., Veilleux S., Mazzarella J. M. 1998, *ApJ*, 492, 116
 Zepf S. E., Ashman K. M. 1993, *MNRAS*, 264, 611

Figure 1. Comparison of the positions of SSCs detected in the optical (Shaya et al. 1994; filled circles) and near-infrared (Scoville et al. 1998; open circles) images. The left upper panel shows the positions taken directly from both of these papers and the left, lower panel is a close up of the central region. The contours show the radio continuum image at 4.83 GHz taken from Baan & Haschick (1995). In the right, upper panel, the near-infrared image is rotated by 4 degree clockwise as described in the text. The right, lower panel again shows a close up of the central region.

Figure 2. Comparisons of the observed optical and near-infrared SEDs (filled circles) with those of best-fit models (dotted lines mean ISB model and dashed lines mean CSF model; see the text and Table 1 for details) for the six SSCs analyzed in this paper. The six points on the SED come from broadband *VRIJHK* measurements. The V band points are all upper limits for the nuclear clusters.

Figure 3. Summary of the plausible parameters of SSCs in the centre of Arp 220 on A_V - age plane. The shaded region is that allowed by SED fitting at the 99 % confidence level. The dashed lines in (a) and (d) represent masses of $1 \times 10^9 M_\odot$, as described in the text. The region to the left of this line is permitted. The dotted lines in (a) - (f) show the epoch when the strength of CO index equal to 0.20 mag for CSF model and ISB model. The region between these two lines is permitted.

Figure 4. Comparison of the observed near-infrared SED of N4 (filled circles) with the best-fit model SED. Dashed line is the best-fit CSF model whose age is 1.0×10^7 yr and the value of A_V is 12.2 mag. Dotted line is the best-fit ISB model whose age is 1.7×10^7 yr and the value of A_V is 12.0 mag.

Table 1. Derived physical properties of the SSCs

SSC	ID ^a	ID ^b	SED type	Age (10 ⁷ y)	A _V (mag)	M _* ^c (M _⊙)	L _{bol} ^d (L _⊙)
N1	1	W	CSF	10	10.8	6.6 × 10 ⁸	9.8 × 10 ¹⁰
N2	3	S	CSF	10	8.4	6.7 × 10 ⁷	1.0 × 10 ¹⁰
N3	2	NE	CSF	10	11.4	2.5 × 10 ⁸	3.6 × 10 ¹⁰
N1	1	W	ISB	1	8.6	8.2 × 10 ⁷	2.4 × 10 ¹⁰
N2	3	S	ISB	1.3	7.6	2.2 × 10 ⁷	4.3 × 10 ⁹
N3	2	NE	ISB	1.3	10.8	7.9 × 10 ⁷	1.6 × 10 ¹⁰
C1	11	4	ISB	0.08	0.4	1.1 × 10 ⁵	1.7 × 10 ⁸
C2	9	1	ISB	2.8	0.4	6.9 × 10 ⁵	5.4 × 10 ⁷
C3	10	2	ISB	3.8	0	3.5 × 10 ⁵	1.9 × 10 ⁷

^a Identifications in Shaya et al. (1994).

^b Identifications in Scoville et al. (1998).

^c Stellar mass of SSCs.

^d Extinction-corrected bolometric luminosity of SSCs

Figure A1. The effect on the SEDs of dust within the SSCs, computed from the onion-skin model described in the text. The solid line is the SED of an SSC with an age of 80 Myr for ISB model. The dotted line is the SED corrected using only a screen model with a line-of-sight extinction $A_{V,s} = 10$. The other lines represent the models listed in Table A1.

Table A1. Parameters of onion skin model

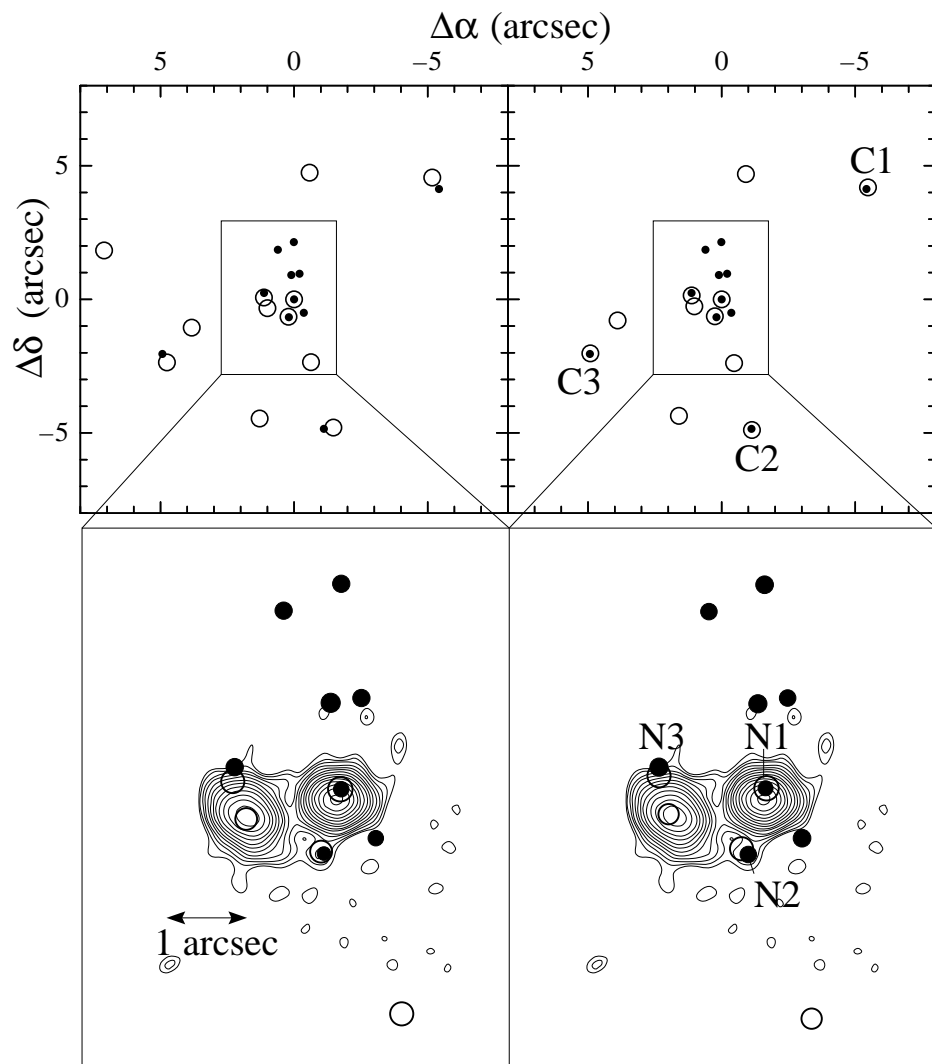
model	$A_{V,s}$	$A_{V,max}$	α
1	0	10	0
2	0	100	0
3	5	100	0
4	10	100	0

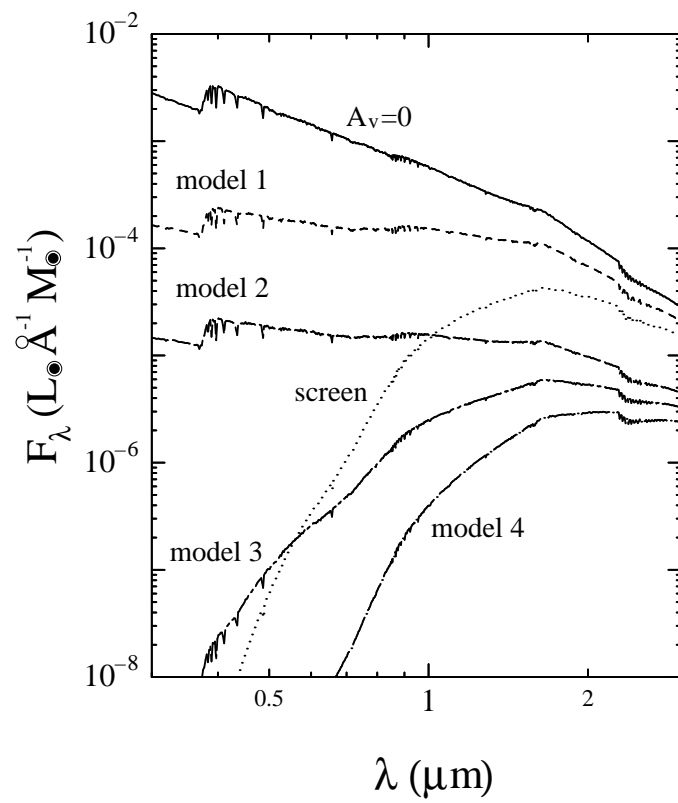
APPENDIX A: ONION-SKIN MODEL OF EXTINCTION

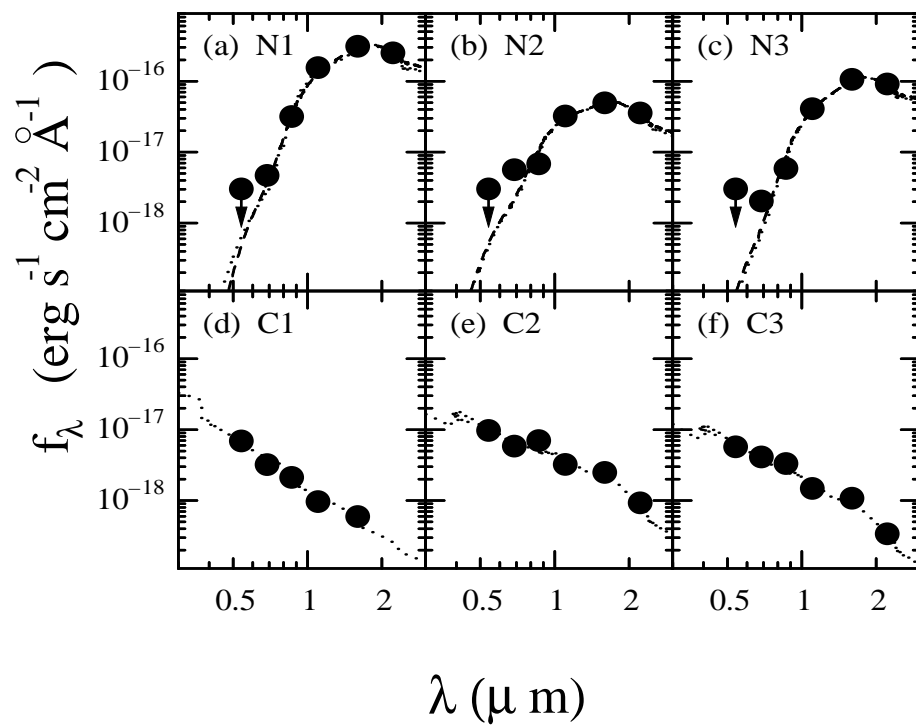
Throughout this work we have used a screen model to quantify extinction by dust. This assumes that all of the dust responsible for the extinction is distributed within Arp 220 between the SSCs and the observer, along our line of sight. This model is inadequate if the SSCs themselves possess significant amount of dust, and we investigate this possibility using the onion-skin model of Surace & Sanders (1999). In that model, to model the effect of mixed stars and dust, a distribution of the unreddened luminosity L_{A_V} obscured by a given line-of-sight extinction A_V is assumed to be a power-law form; $L_{A_V} = L_{A_V=0}(A_V + 1)^\alpha$. The amount of internal extinction from within the SSC is therefore parameterised by two numbers: $A_{V,max}$, which is a maximum value of A_V , and α , which is a parameter modeling the distribution of dust within the SSCs (the case $\alpha = 0$ corresponds to a scenario in which the dust and stars are well mixed; this is the case that we are worried about here). Figure A1 shows the SEDs of SSCs for some of these models; the relevant parameters are presented in Table A1. Here $A_{V,s}$ is the extinction from a screen component unassociated with the SSCs that is superimposed on the internal extinction.

The most important thing that we infer from the figure is that the shape of the SED is determined primarily by the foreground extinction. Were extinction from dust within the clusters to be the more important, we would expect a far higher visible-to-near-infrared flux ratio than is observed. Our use of the screen model in the SED fitting is therefore reasonable.

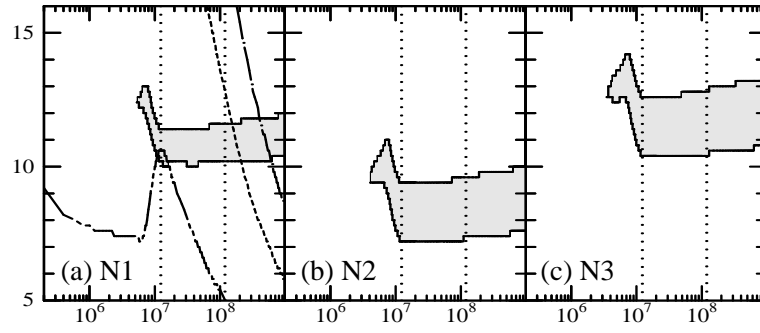
It is important to note, however, that, although the shapes of the SEDs are similar (compare the model 4 with the screen model), the flux of the well-mixed+screen model is smaller than that of the pure-screen model. This is because the stars with a large local A_V do not contribute to the global SED of the SSC at visible and near-infrared wavelengths. Therefore the SSC luminosities evaluated in the main body of the paper are formally lower limits because of this danger of there existing very heavily obscured regions *within* the SSCs. These very-heavily obscured regions could be responsible for a substantial part of the bolometric luminosity of the SSCs or even the whole galaxy. Operationally, as far as the spectral energy distributions are concerned, these regions behave exactly like very-heavily obscured regions *outside* the SSCs, for example at the galaxy nucleus, as they have no measurable signature at the wavelengths studied here.







CSF



ISB

